Contrib Mineral Petrol (1995) 121:201–216

T.P. Wagner · J.M. Donnelly-Nolan · T.L. Grove

Evidence of hydrous differentiation and crystal accumulation in the low-MgO, high-Al_2O_3 Lake Basalt from Medicine Lake volcano, California

Received: 10 May 1994 / Accepted: 12 February 1995

Abstract The late Pleistocene Lake Basalt of Medicine Lake volcano, California is comprised of variably porphyritic basalt and basaltic andesite flows and scoria. These eruptives are similar in composition and phenocryst abundance to the low-MgO, high-Al_2O_3 mafic magmas common in convergent margin settings. The petrogenesis of the magmas that produced the Lake Basalt has been inferred from field relations, melting experiments and subsequent major and trace element modeling. Their formation involved both hydrous differentiation and plagioclase accumulation and thus the Lake Basalt can be used to constrain the relative contributions of these processes to the production of high-Al_2O_3 arc basalt. Phenocryst-poor lavas of the Lake Basalt formed by hydrous differentiation; their compositions and observed phenocrysts were reproduced in 1 kbar, H_2O-saturated melting experiments. Anorthite-rich plagioclase compositions of the lavas of the Lake Basalt necessitate crystallization from melts with between 4 and 6 wt% dissolved H_2O. Phenocryst-rich lavas of the Lake Basalt, with 18 modal% phenocrysts and greater, formed by plagioclase accumulation in magmas similar to the phenocryst-poor lavas. This interpretation is supported by the depleted incompatible element abundances and enriched Sr/Zr ratio of the more porphyritic lavas relative to the phenocryst-poor lavas. We model the formation of the Lake Basalt as a two-stage process that combines a differentiation model and a plagioclase accumulation model. Stage one involved hydrous fractionation, granitic assimilation and mixing with undifferentiated parent magma. This process generated lavas with up to 19.2 wt% Al_2O_3 and 7 modal% phenocrysts. In stage two, plagioclase accumulated in these liquids and produced more aluminous and porphyritic lavas with up to 21.8 wt% Al_2O_3 and 33 modal% phenocrysts.

T.P. Wagner (✉) · T.L. Grove
Department of Earth, Atmospheric and Planetary Science,
Massachusetts Institute of Technology,
Cambridge, MA 02139, USA

J.M. Donnelly-Nolan
U.S. Geological Survey,
345 Middlefield Road, Menlo Park, CA 94025, USA

Editorial responsibility: I.S.E. Carmichael

Introduction

Low-MgO high-Al_2O_3 basalt (low-MgO HAB) and basaltic andesite (BA) are among the dominant products of arc volcanism. They are thought to be derived from melts of the mantle wedge located above subducted oceanic slabs (Boettcher 1973; Ringwood 1974). Melting of the wedge is fluxed by dehydration of the downgoing slab, which produces magmas that are notably more water-rich than those generated in other tectonic settings. Mantle melts are more magnesian and less aluminous than low-MgO HABs and BAs and must undergo significant compositional modification prior to eruption. Modification by differentiation is supported by some studies of the lavas' compositional variation and hydrous experimental work. The melting experiments of Sisson and Grove (1993a,b) show that typical low-MgO HABs and BAs can be produced by crystallization of mantle melts with dissolved H_2O contents of 4 to 6 wt%. There are, however, good reasons to question whether all low-MgO HABs and BAs are liquids. These lavas can have very high abundances of phenocrysts that have textures and compositional zonation indicative of disequilibrium conditions. Noting these and other geochemical characteristics of HABs, Crawford et al. (1987) proposed that these lavas have accumulated plagioclase phenocrysts and are not liquid compositions produced by crystallization.

The Lake Basalt of Medicine Lake volcano (MLV) falls within the compositional range of typical low-MgO HABs and BAs from the Aleutian Islands, Central America and elsewhere. Lavas of the Lake Basalt offer insight into the question of liquid versus cumulate origin of low-MgO HABs and BAs because they are variably porphyritic and show clear genetic relationships between nearly aphyric and phenocryst-rich lavas. We have com-

bined an experimental melting study with major and trace element modeling to constrain the roles of crystal fractionation and crystal accumulation in their formation.

Geologic setting and field relations

Medicine Lake volcano is a large Pleistocene and Holocene shield volcano in the southern Cascade Range with an estimated volume of 750 km^3 (Donnelly-Nolan et al. 1990; Dzurisin et al. 1991). The eruptive products range from primitive high-alumina basalt to rhyolite. The Lake Basalt was identified by Powers (1932, pp 262–263) as a coherent group of eruptive materials and later mapped and described by Anderson (1941, pp 364–365, 388). Remapping combined with chemical analyses and paleomagnetic measurements (J. Donnelly-Nolan and D.E. Champion, unpublished data 1980–1993) shows that the unit includes porphyritic and less phyric lavas that cover a large area of the volcano's eastern rampart and southeastern flank, as well as the type locality within the caldera of MLV. Late Pleistocene glaciation and subsequent eruptions have covered and obscured some of the contact relations making a detailed discrimination of flow units and an eruptive sequence impossible. Lavas comprising the Lake Basalt cover an area of approximately 150 km^2 (Fig. 1); assuming an average thickness of 20 m, their estimated volume is 3 km^3. Outcrops of the Lake Basalt are commonly scoriaceous and even where massive are purplish in hue because of pervasive oxidation. The lavas erupted from multiple vents, most forming a 15 km long, NNW trending array that is similar to other regional vent and fault trends. These are among the highest cinder cones at MLV, including 500 m high Border Mountain. Three vents lie within the caldera and form an approximate E-W trend, intersecting the NNW trend at its northern end (Fig. 1).

The lavas are subdivided by mapping into four major groups: Caldera, North, South and less porphyritic (Fig. 1). The Caldera, North and South group lavas are highly porphyritic and contain 7 to 33 modal% phenocrysts. The less porphyritic lavas contain less than 3 modal% phenocrysts and are relatively rare. Field relations and paleomagnetic data indicate that the events which formed the Lake Basalt began with the eruption of the Caldera group. The lavas of the Caldera group stratigraphically underlie the rest of the lavas of the Lake Basalt with flows exposed both inside and outside the caldera rim. The lavas erupted from the E-W trend of vents and one or more sources (now buried) in the vicinity of Red Shale Butte and Lyons Peak. The eruption of the Caldera group was followed by a hiatus of geologically short duration, after which the NNW trending vents opened and erupted the lavas of the North and South groups. In the area of the North group, the event began and ended with eruption of the less porphyritic lavas that are exposed within and on its boundaries. The less porphyritic lavas are here subdivided into two subgroups based on their location and inferred eruptive sequence, early or late. The early less porphyritic lavas form flows exposed along the eastern and southwestern margin of the North group. The late less porphyritic magmas erupted as spatter at the top of three vents for the North group: Red Shale Butte, Lyons Peak and the vent SE of Lyons Peak. Each of these three vents has a base of more porphyritic spatter which grades upward into the less porphyritic facies with no observable discontinuity. This sequence of alternating more and less porphyritic magma facies is similar to that described by Rose et al. (1978) for Fuego volcano in Guatemala.

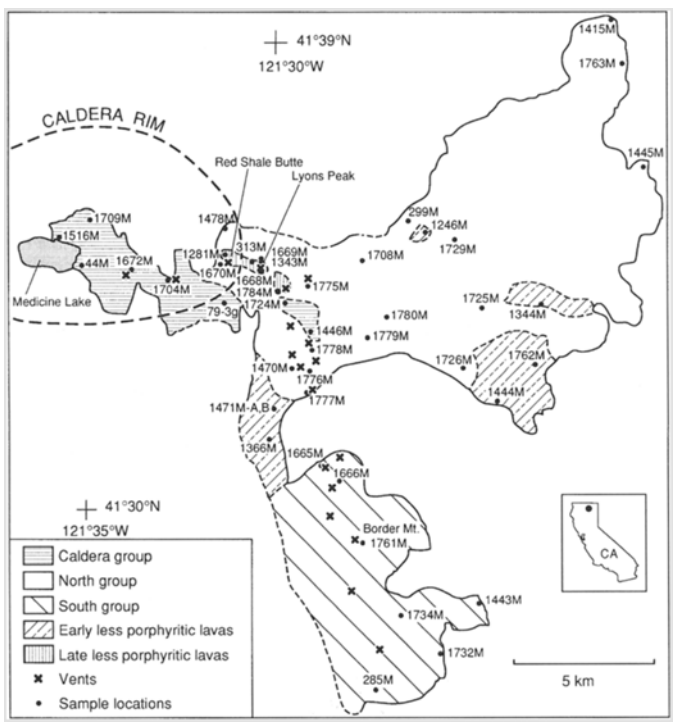

Fig. 1 Location map shows distribution of the Lake Basalt. *Dashed lines* are inferred or approximate boundaries. Inset map shows location within state of California, USA

Analytical methods

Whole rock samples were ground to powders in alumina and analyzed for major elements by X-ray fluorescence spectrometry at the U. S. Geological Survey laboratory in Lakewood, Colorado. Analytical methods and estimates of precision are discussed by Taggart et al. (1987). Splits of selected samples were analyzed for the rare earth elements, Cr, Co, Cs, Hf, Ta, Th and U concentrations by Instrumental Neutron Activation Analysis (INAA) at the U. S. Geological Survey laboratories at Lakewood, Colorado and Reston, Virginia. Rb, Sr, Y, Zr, Nb, Ba, Ni, Cu, Zn and Cr concentrations were measured by energy dispersive X-ray fluorescence techniques at the U. S. Geological Survey in Menlo Park, California. See Baedecker (1987) for description of the analytical technique. All data are reported in Table 1.

Lava phenocrysts and the experimental products were analyzed by electron microprobe at MIT on a JEOL 733 Superprobe using wavelength-dispersive techniques. Data were reduced using the correction scheme of Bence and Albee (1968) with the modifications of Albee and Ray (1970). Crystalline phases in the lavas and experiments were analyzed at 15 kV accelerating potential, 10 nA beam current and a spot size on the order of 2 μm. Spot size was increased to 30 μm to analyze the hydrous glasses in the experiments. The large spot sizes and low beam currents were used to minimize diffusion of alkali elements away from the region of interest during the analysis. The H_2O content of the experimental glasses was estimated from the electron microprobe analyses by summation deficit. This technique has been shown to produce results within ± 0.2–0.3 wt% to those obtained by ion microprobe techniques (Sisson and Layne 1993). Electron microprobe analyses were corrected for analytical bias relative to the XRF major element data, +5% for TiO_2 and −9.6% for Na_2O. Values were determined by comparing the concentration of these elements in experiment 15 to the XRF analysis of 1471M-B.

Petrography and chemical composition of the lavas

The lavas show a complete gradation in phenocryst abundance and range from nearly aphyric to highly porphyritic with 33 modal% phenocrysts. Highly porphyritic lavas grade into nearly aphyric lavas with no observable discontinuity at a number of vent areas for

Table 1a Major element contents of the lavas of the Lake Basalt (wt%, normalized to 100 excluding LOI), determined at USGS, Lakewood, CO (analysts J. Baker, A. Bartel, J. Mee, D. Siems, J. Taggart, J. Wahlberg)

Sample	SiO_2	Al_2O_3	FeO[a]	MgO	CaO	Na_2O	K_2O	TiO_2	P_2O_5	MnO	Total[b]	LOI[c]
Less porphyritic – Early												
1246 M	55.1	17.5	8.02	4.71	8.54	3.80	0.86	1.12	0.24	0.14	100.2	0.27
1344 M	54.8	17.9	7.88	4.50	8.90	3.64	0.93	1.11	0.23	0.14	100.0	0.39
1366 M	51.5	18.2	9.16	5.92	9.87	3.39	0.44	1.17	0.18	0.16	100.3	0.10
1444 M	52.8	18.0	8.50	5.50	9.80	3.41	0.62	1.11	0.18	0.15	100.0	0.44
1471 M-B	52.1	17.9	9.03	5.98	9.70	3.44	0.48	1.13	0.18	0.16	100.7	<0.01
1762 M	53.7	18.1	8.08	5.14	9.43	3.37	0.80	1.06	0.21	0.15	99.8	0.16
1778 M	55.3	17.6	8.04	4.44	8.36	3.84	0.85	1.18	0.25	0.14	99.4	0.25
1784 M	55.5	17.7	7.80	4.51	8.30	3.86	0.87	1.13	0.24	0.14	99.4	0.34
Less porphyritic – Late												
313 M	55.7	17.5	8.06	4.28	8.21	3.82	0.85	1.14	0.23	0.14	99.6	0.31
1281 M	53.7	17.9	8.34	5.46	9.04	3.54	0.56	1.12	0.22	0.15	100.8	0.13
1343 M	54.5	18.0	7.90	4.83	8.80	3.70	0.71	1.10	0.23	0.14	100.1	0.25
1668 M	56.1	17.4	7.81	4.32	7.93	3.86	1.00	1.12	0.25	0.14	99.0	0.35
More porphyritic – Caldera group												
44 M	50.6	21.4	8.16	4.12	10.65	3.15	0.50	1.08	0.17	0.13	100.4	0.14
79 3g	50.4	21.2	8.27	4.21	10.60	3.41	0.48	1.12	0.21	0.14	100.0	<0.01
1446 M	50.0	21.6	8.10	4.18	11.05	3.27	0.42	1.07	0.17	0.13	100.5	0.03
1516 M	50.1	21.4	8.13	4.28	10.92	3.28	0.47	1.07	0.18	0.13	100.7	<0.01
1672 M	50.0	21.7	8.11	4.32	10.86	3.19	0.44	1.08	0.18	0.14	99.4	<0.01
1704 M	50.3	21.5	8.18	4.13	10.78	3.29	0.47	1.11	0.19	0.14	100.2	<0.01
1709 M	51.0	21.3	7.97	4.11	10.35	3.32	0.58	1.07	0.20	0.14	100.4	0.09
1724 M	50.1	21.7	8.04	4.16	10.82	3.28	0.45	1.07	0.20	0.14	100.7	<0.01
More porphyritic – North group												
299 M	53.0	21.1	6.51	4.08	10.10	3.23	0.70	0.91	0.19	0.11	99.7	0.05
1415 M	54.0	19.7	6.97	4.05	9.56	3.49	0.85	1.02	0.23	0.12	99.7	0.34
1445 M	52.8	20.6	6.64	4.71	10.33	3.20	0.63	0.85	0.19	0.11	100.4	0.30
1470 M	51.0	20.8	7.28	5.06	11.07	3.10	0.41	0.92	0.16	0.12	100.2	0.10
1471 M-A	51.5	19.2	8.35	5.64	10.33	3.27	0.44	1.04	0.17	0.15	100.6	<0.01
1478 M	52.4	19.8	7.42	5.02	10.15	3.37	0.50	0.98	0.18	0.13	100.4	0.22
1669 M	53.1	19.1	7.74	5.19	9.46	3.43	0.60	1.04	0.21	0.14	99.3	0.19
1670 M	52.5	18.9	8.35	5.16	9.60	3.45	0.57	1.13	0.21	0.15	99.4	0.15
1708 M	53.1	20.9	6.55	4.13	9.93	3.42	0.65	0.94	0.23	0.12	100.0	<0.01
1725 M	54.6	18.6	7.75	4.33	8.79	3.53	0.91	1.09	0.25	0.14	99.9	0.39
1726 M	51.0	20.9	7.50	5.17	10.67	3.09	0.38	0.96	0.19	0.14	100.1	<0.01
1729 M	53.3	20.2	6.89	4.65	9.69	3.46	0.60	0.91	0.22	0.13	100.3	<0.01
1763 M	54.2	19.7	7.15	4.06	9.19	3.47	0.77	1.06	0.25	0.13	99.1	0.51
1775 M	52.9	21.0	6.59	4.19	9.97	3.41	0.67	0.96	0.21	0.12	99.0	0.25
1776 M	52.3	21.5	6.28	4.66	10.52	3.11	0.55	0.82	0.18	0.11	99.5	0.2
1777 M	52.4	21.4	6.39	4.34	10.66	3.05	0.61	0.86	0.18	0.11	99.2	0.34
1779 M	52.5	21.3	6.34	4.59	10.49	3.11	0.61	0.83	0.19	0.11	99.8	0.11
1780 M	51.7	21.8	6.49	4.76	10.64	3.05	0.48	0.84	0.19	0.12	99.4	0.3
More porphyritic – South group												
285 M	51.2	21.0	7.39	5.21	10.70	2.91	0.39	0.94	0.16	0.13	99.9	0.28
1443 M	51.1	20.8	7.23	5.28	10.87	2.98	0.45	0.92	0.17	0.12	100.1	0.28
1665 M	50.8	21.8	6.67	5.10	11.27	2.90	0.39	0.82	0.14	0.12	99.2	0.36
1666 M	51.9	20.2	7.58	5.14	10.15	3.21	0.52	1.00	0.20	0.14	99.4	0.09
1732 M	50.4	21.7	7.21	5.25	10.93	3.04	0.26	0.90	0.19	0.13	99.6	0.12
1734 M	50.4	21.5	7.25	5.40	10.91	2.96	0.33	0.91	0.18	0.13	99.8	0.04
1761 M	51.9	21.6	6.36	4.91	10.56	3.00	0.52	0.80	0.19	0.12	100.1	0.19

[a] Total iron calculated as FeO
[b] Total is the original total with Fe as Fe_2O_3 plus LOI
[c] LOI is loss on ignition at 900° C

the North group. Anorthite-rich plagioclase is the most abundant phenocryst, followed by much less common olivine (Table 2). Minor amounts of high-chromium spinel and titanomagnetite phenocrysts are present in most samples, while clinopyroxene phenocrysts are found in only one sample. Groundmass in all samples is completely crystalline and contains microphenocrysts of plagioclase, olivine, clinopyroxene and magnetite.

Plagioclase phenocrysts vary from large equant laths to broken and resorbed crystals and range in size from 0.2 to 3.5 mm. Some phenocrysts have sieve-like textures due to large numbers of inclusions of groundmass material. Many phenocrysts have rims of more albitic plagioclase up to 10 μm thick. Phenocryst core compositions are both normally and inversely zoned and vary from An_{62} to An_{87} with rims from An_{43} to An_{47} (Table 3; Anderson

Table 1b Neutron activation trace element (ppm) contents of the lavas of the Lake Basalt, determined by INAA at USGS, Lakewood, CO (analysts J. Budahn and R. Knight) and Reston, VA (analysts P. Baedecker, J. Mee and G. Wandless) – (not determined)

Sample	Sc	Cr	Co	Cs	La	Ce	Nd	Sm	Eu	Tb	Yb	Lu	Hf	Ta	Th	U
Less porphyritic – Early																
1246 M	28.4	64	26.5	0.72	11.1	22.9	13.0	3.54	1.200	0.530	1.90	0.280	2.3	0.24	1.70	<1.20
1344 M	28.9	66	26.3	0.74	10.8	23.3	13.0	3.47	1.240	0.540	1.97	0.290	2.4	0.25	1.65	0.420
1366 M	35.0	104	35.4	0.42	8.20	18.6	12.1	3.41	1.170	0.600	2.41	0.350	2.4	0.18	0.86	<0.80
1471 M-B	33.6	101	34.6	–	7.9	18.4	10.5	3.29	1.170	0.582	2.76	0.398	2.37	0.205	0.99	0.350
1762 M	33.7	109	31.1	0.75	9.97	20.6	11.3	3.52	1.190	0.567	2.11	0.327	2.5	<0.3	1.89	0.550
1784 M	28.5	63	25.7	0.75	10.8	23.6	13.2	3.62	1.230	0.568	1.96	0.278	2.62	0.339	1.90	0.640
Less porphyritic – Late																
313 M	28.3	49	24.5	0.77	10.8	26.7	14.8	3.55	1.270	0.551	1.77	0.315	2.58	0.235	1.73	–
1281 M	30.2	85	30.4	0.54	11.1	22.9	15.0	3.66	1.250	0.570	2.00	0.320	2.2	0.20	1.20	<1.40
1343 M	27.9	72	27.6	0.66	10.5	22.4	13.5	3.40	1.210	0.530	1.80	0.258	2.34	0.24	1.55	0.450
1668 M	28.1	55	25.4	0.95	12.4	25.6	14.4	3.56	1.310	0.620	2.16	0.312	2.88	0.342	2.32	0.740
More porphyritic – Caldera group																
44 M	22.7	46	26.3	0.36	6.2	13.5	9.0	2.31	1.060	0.449	1.79	0.278	1.70	0.160	0.82	–
79 3g	25.9	55	29.0	0.24	7.12	15.1	10.2	3.09	1.140	0.513	1.92	0.281	2.05	0.194	0.74	0.310
1672 M	26.3	57	31.3	0.32	7.33	16.2	10.8	3.07	1.180	0.551	1.98	0.286	2.09	0.2	0.84	0.250
1704 M	24.2	51	27.7	0.24	6.56	14	8.7	2.76	1.080	0.480	1.72	0.252	1.8	0.18	0.83	0.184
1709 M	24.0	53	28.0	0.59	7.45	15.9	9.4	3.12	1.110	0.510	1.84	0.280	2.07	0.208	1.17	0.430
1724 M	23.8	53	27.8	0.23	6.25	14	9.1	2.86	1.090	0.498	1.72	0.244	1.84	0.185	0.66	0.252
More porphyritic – North group																
299 M	19.7	59	21.4	0.56	7.6	17.3	10.7	2.59	1.020	0.417	1.39	0.214	1.90	0.231	1.21	–
1471 M-A	30.4	98	32.0	0.28	7.4	16.0	11.3	2.98	1.080	0.520	2.14	0.298	2.05	0.178	0.83	0.240
1669 M	28.6	86	30.1	0.41	8.8	19.6	11.9	3.21	1.160	0.533	1.87	0.264	2.13	0.221	1.20	0.390
1670 M	32.4	82	31.9	0.51	9.3	21.3	13.0	3.29	1.260	0.593	2.24	0.319	2.45	0.224	1.23	0.320
1763 M	23.7	59	23.5	0.64	10.5	21.8	12.5	3.39	1.150	0.494	1.65	0.252	2.34	0.306	1.65	0.660
1775 M	21.6	72	23.4	0.51	9.48	19.9	12.4	2.96	1.080	0.446	1.52	0.222	2.14	0.289	1.37	0.500
1776 M	20.9	81	25.2	0.45	7.84	17.2	10.8	2.54	0.947	0.388	1.39	0.191	1.69	0.182	1.11	0.330
More porphyritic – South group																
1443 M	25.4	89	29.5	0.28	7.26	15.9	9.4	2.82	1.008	0.432	1.63	0.243	1.73	0.179	0.83	0.260
1665 M	25.0	141	28.2	0.4	7.42	15.4	9.1	2.67	0.937	0.446	1.63	0.233	1.81	0.193	1.33	0.450
1761 M	20.7	84	26.3	0.35	7.59	16.3	9.7	2.45	0.955	0.362	1.29	0.185	1.62	0.145	1.11	0.330

1941; Gerlach and Grove 1982). Olivine phenocrysts have broken, sharp edges and range in size from 0.2 to 0.9 mm. Olivines are generally homogeneous in composition within each sample, though some cores are slightly normally zoned. Phenocryst core compositions throughout the suite vary from Fo_{70} to Fo_{82}. Thin rims (<5 μm) of more fayalitic olivine (Fo_{64} to Fo_{77}) are present on some phenocrysts. Spinels are found as individual phenocrysts and inclusions in olivine and plagioclase and range in size from 0.04 to 0.18 mm. They vary in composition from titanomagnetite to high-chromium spinel (Cr-sp). Titanomagnetites are generally equant in shape and are found as phenocrysts and inclusions. Cr-sp are rarer than titanomagnetites and have rounded and embayed edges where present in the groundmass but can be equant as inclusions. Their molar $^{Cr}/_{Cr+Al}$ varies from 40 to 74; the most chromium-rich spinels are present only as inclusions. Clinopyroxene forms phenocrysts in only one sample (1709M), where it is present in glomerocrystic intergrowths with olivine and plagioclase.

The map units comprising the Lake Basalt (Fig. 1) correlate with compositional and modal phenocryst abundance differences (Fig. 2, Table 2). Whole-rock Al_2O_3 contents correlate with plagioclase phenocryst abundances, as observed by Ewart (1982) and Crawford et al. (1987) for other arcs. The less porphyritic units have the lowest Al_2O_3 contents (17.4 to 18.2 wt%) and the lowest plagioclase phenocryst abundances (<2.3 modal%). The Caldera and South group lavas have the highest Al_2O_3 contents (>20 wt%) and the highest plagioclase phenocryst contents. The South group lavas have higher MgO contents than the Caldera group lavas due to their greater abundance of olivine phenocrysts. The North group lavas have the largest compositional variation and correspondingly show the largest variations in phenocryst abundance, ranging from the least to most porphyritic.

Experimental methods

Starting composition

A sample of the less porphyritic lavas with the highest Mg# (100^*molar $^{MgO}/_{MgO + FeO}$ = 54), 1471M-B, was chosen as a starting composition. It contains only trace amounts of olivine and plagioclase phenocrysts and is thus likely to represent a liquid composition. A split of the powder used for chemical analysis was reground under ethyl alcohol in an agate mortar to reduce the grain size.

Experiments

All experiments were performed in a TZM rapid quench pressure vessel using the assembly and techniques described in Sisson and Grove (1993a). Sample powder was placed in a 0.25" × 0.15" cylindrical Au sample capsule which was crimped and welded closed on one end and simply crimped and left unsealed on the other. This sample capsule was loaded into a 1" × 0.20" cylindrical Au outer capsule with 2 or 3 Pt buffer capsules and approximately 18 μl of H_2O. The Pt buffer capsules contained a mixture of Ni and NiO. The outer capsule was sealed by welding at each end. The sample and Pt buffer capsules were left unsealed to allow for O_2 exchange. The highest temperature experiment exceeded the melting point of Au; in this case, Au_{80}-Pt_{20} and Ag-Pd alloys were substituted for the outer capsule and sample capsules respectively. Fe loss to the Au and Ag-Pd sample capsules is negligible; mass balance of all observed phases against the starting composition showed Fe to balance within 1% relative.

Table 1c XRF trace element (ppm) contents of the lavas, determined by energy dispersive XRF at USGS, Menlo Park, CA (analyst P. Bruggman); 313 M values determined by wavelength dispersive XRF at USGS, Reston, VA (analysts D. Burgi and R. Johnson) (– not determined)

Sample	Rb	Sr	Y	Zr	Nb	Ba	Ni	Cu	Zn	Cr
Less porphyritic – Early										
1246 M	19	601	23	120	6	363	25	80	80	–
1344 M	24	590	24	122	4	351	26	72	54	67
1366 M	13	502	27	113	5	262	48	84	59	109
1444 M	17	459	30	108	6	322	45	95	68	104
1471 M-B	15	487	29	104	5	206	51	77	67	86
1762 M	23	477	32	120	8	350	32	72	72	103
1778 M	16	590	18	120	–	390	24	85	78	64
1784 M	14	610	17	122	–	400	18	77	72	66
Less porphyritic – Late										
313 M	25	592	19	115	5	377	–	–	–	–
1281 M	11	602	21	104	2	365	40	65	80	–
1343 M	21	578	23	110	6	317	36	46	59	71
1668 M	27	587	29	135	7	383	26	74	84	69
More porphyritic – Caldera group										
44 M	13	522	20	102	4	281	33	59	43	38
79 3g	10	550	20	92	–	280	–	–	–	–
1446 M	12	555	28	106	6	280	45	57	52	49
1516 M	9	531	20	93	2	256	28	62	63	34
1672 M	12	549	21	102	3	291	34	72	67	68
1704 M	23	563	29	107	5	254	27	79	66	51
1709 M	16	561	25	111	6	271	32	65	66	55
1724 M	10	557	25	103	4	233	25	54	71	48
More porphyritic – North group										
299 M	17	688	17	110	5	308	23	–	59	–
1415 M	22	665	28	117	5	317	32	54	58	50
1445 M	14	655	24	96	5	274	49	48	57	82
1470 M	12	627	27	89	6	205	51	55	52	79
1471 M-A	18	543	26	99	5	192	50	74	53	79
1478 M	23	681	27	106	6	284	48	61	48	72
1669 M	20	632	26	109	6	299	38	57	66	88
1670 M	21	598	26	114	6	268	44	72	71	93
1708 M	13	710	22	112	8	312	34	64	61	70
1725 M	24	627	26	124	6	317	28	81	67	63
1726 M	19	656	30	101	6	203	46	74	67	78
1729 M	20	705	25	108	4	302	37	58	59	74
1763 M	24	674	25	125	8	342	20	63	69	58
1775 M	14	720	18	104	–	340	31	61	61	–
1776 M	12	730	15	85	–	310	38	53	54	83
1777 M	10	730	14	87	–	290	29	60	52	81
1779 M	11	730	15	82	–	285	36	57	58	62
1780 M	11	730	15	85	–	290	46	56	53	79
More porphyritic – South group										
285 M	9	625	15	96	7	214	65	57	47	84
1443 M	13	675	26	99	6	228	63	57	44	82
1665 M	13	550	21	89	2	323	52	76	50	119
1666 M	13	647	22	102	4	274	43	73	67	88
1732 M	9	670	21	90	4	226	59	63	60	87
1734 M	13	663	23	92	4	218	64	62	56	106
1761 M	22	759	24	99	6	241	55	54	55	82

All experiments were performed at 1 kbar, using a mixture of argon and methane (CH_4) gas added in the proportion of 2000 psi:20 psi as the pressure medium. The breakdown of CH_4 to graphite and H_2(gas) slows H_2 diffusion out of the outer capsule and helps maintain its H_2O content. An experiment was judged successful on the basis of the following criteria: (1) liquid H_2O was present upon puncture of the outer capsule, (2) buffer capsules contained both Ni and NiO and (3) silicate liquid formed a glass free of quench growth. Individual run conditions and phase proportions are reported in Table 4. Phase compositions for each experiment are reported in Table 5.

Matrix separates

The matrix material in two of the more porphyritic samples, 1443M (South group) and 79–3g (Caldera group) was separated for chemical analysis. Rocks were coarsely crushed (0.5 to 2 mm in size) in a platener mortar and the least phyric pieces were hand separated under a binocular microscope. The samples were ground in an agate mortar and completely melted in gold capsules under H_2O saturated conditions at 1.75 kbar and 1050°C. Compositions of the resultant glasses were determined by electron microprobe. Higher pressures were used than in the experiments to increase the sample water content and ensure complete melting.

Experimental results

The liquid phase in all experiments quenched to a hydrous, homogeneous glass with approximately 4–5 wt% H_2O. The glass compositions define a differentiation trend that ranges from low-MgO HAB to andesite, characterized by increasing SiO_2, Na_2O and TiO_2 with decreasing Al_2O_3, CaO and MgO contents (Fig. 2). These trends are similar to those defined by the less porphyritic lavas of the Lake Basalt. Al_2O_3 contents of the experimental liquids range from 17.1 to 18.1 wt% and are thus distinctly lower than many low-MgO HAB. Olivine (ol) is the liquidus phase near 1075°C, joined within a 25° reduction in temperature by plagioclase (pl) and chrome-spinel (Cr-sp). Cr-sp is only present in trace amounts. Ol, pl and Cr-sp crystallize together until 1030°C, where high-calcium pyroxene (cpx) joins the assemblage at the expense of Cr-sp. Titanomagnetite appears at 1000°C.

Olivine

The olivines in all experiments are homogeneous in composition and equant in shape. The Fe/Mg exchange K_D [$K_D = (Fe_{ol}/Mg_{ol})/(Fe_{liq}/Mg_{liq})$] ranged from 0.27 to 0.30 with an average value of 0.29 ± 0.01, assuming all Fe is Fe^{2+}. Sisson and Grove (1993a) measured $Fe^{3+}/(Fe^{2+} + Fe^{3+})$ to be 0.137 by Mossbauer spectroscopy in

Table 2 Modal abundances (vol.%; normalized to 100%, vesicle free)

Group	Sample	Groundmass	Plagioclase	Olivine	Spinel	# of Points
Less Porph.	1366 M	97.7	2.3	tr	tr	1143
North	1471 MA	93.5	5.9	0.5	0.1	2140
North	1763 M	82.7	16.4	1.0	tr	1065
Caldera	1516 M	66.7	32.7	0.5	tr	1808
Caldera	79-3g	70.0	29.4	0.6	tr	1183
South	1443 M	74.1	24.2	1.7	tr	1112

Table 3 Phenocryst compositions of the lavas of the Lake Basalt (*nd* not detected, – not determined)

Phase	Pts.	SiO_2	TiO_2	Al_2O_3	Cr_2O_3	FeO	MgO	MnO	CaO	K_2O	Na_2O	Fe_2O_3	Sum	Mg# or An#
1366 M Less porphyritic														
Ol-core	8	39.2	0.1[b] nd	0.06 0.01	0.04 0.01	17.5 0.08	42.7 0.1	0.29 0.01	0.21 0.01	–	–	–	100.0	0.81
Ol-rim	1	38.5	0.01	0.04	0.06	21.3	39.4	0.34	0.27	–	–	–	99.9	0.77
Pl-core	1	46.5	–	34.6	–	0.42	0.13	–	17.8	0.02	1.54	–	101.0	0.87
Pl-core	4	49.3 0.8	–	31.8 0.35	–	0.62 0.04	0.16 0.01	–	15.7 0.54	0.05 0.00	2.79 0.33	–	100.4	0.76
Pl-rim	1	51.1	–	31.0	–	0.65	0.17	–	14.0	0.06	3.73	–	101.2	0.67
Sp[a]	1	nd	1.34	25.5	28.4	17.9	12.4	0.33	0.15	–	–	15.0	101.0	
Sp	1	nd	17.7	0.89	0.48	43.0	2.28	0.53	0.36	–	–	34.2	99.5	
1516 M Caldera group														
Ol-core	2	38.7	0.2 nd	0.03 0	0.12 0.01	21.0 0.03	40.3 0.1	0.38 0.01	0.23 0.04	–	–	–	100.8	0.77
Ol-rim	1	37.1	0.10	0.02	0.14	29.2	33.6	0.45	0.29	–	–	–	101.0	0.67
Pl-core	1	48.0	–	32.8	–	0.69	0.11	–	16.7	0.02	2.10	–	100.4	0.81
Pl-core	1	48.8	–	31.7	–	0.74	0.12	–	15.9	0.04	2.60	–	99.9	0.77
Pl-rim	1	55.7	–	27.5	–	0.74	0.14	–	10.8	0.249	5.33	–	100.2	0.53
Sp	1	nd	2.01	20.9	27.8	19.4	11.1	0.38	0.16	–	–	18.5	100.3	
Sp	1	nd	16.1	1.62	3.40	40.8	3.31	0.57	0.12	–	–	34.9	100.8	
1709 M Caldera group														
Ol-core	6	37.1 0.2	0.09 0.01	0.04 0.02	0.07 0.03	26.7 0.5	35.3 0.6	0.43 0.02	0.22 0	–	–	–	100.0	0.70
Pl-core	1	47.2	–	33.2	–	0.56	0.11	–	17.1	0.03	1.67	–	100.0	0.85
Pl-core	1	53.8	–	29.3	–	0.85	0.11	–	12.5	0.11	4.24	–	100.9	0.62
Sp	1	0.16	11.9	4.74	1.22	41.2	0.07	0.33	0.02	–	–	36.2	95.9	
Cpx-Core	6	50.9 0.4	0.76 0.04	3.0 0.3	0.08 0.08	8.8 0.3	15.1 0.2	0.21 0.01	20.8 0.2	–	0.31 0.04	–	100.0	0.75
79-3g Caldera group														
Ol-core	1	36.5	0.03	0.01	nd	26.5	36.24	0.52	0.22	–	–	–	100.0	0.71
Ol-rim	1	36.3	0.05	0.15	nd	31.6	31.8	0.7	0.19	–	–	–	100.9	0.64
Pl-core	1	48.4	–	33.4	–	0.75	0.01	–	16.3	0.07	2.14	–	101.1	0.81
Pl-core	1	49.7	–	31.7	–	0.70	0.03	–	15.2	0.11	2.76	–	100.2	0.75
Pl-rim	1	58.2	–	25.8	–	0.96	0.10	–	8.6	0.59	6.34	–	100.6	0.43
Sp	1	nd	6.63	8.37	11.7	32.7	4.0	0.4	0.06	–	–	37.7	101.5	
Sp	1	nd	27.5	0.66	0.10	52.9	1.1	0.3	0.23	–	–	12.3	95.1	
1443 M South group														
Ol-core	2	39.2 0.3	nd	0.03 0.01	0.01 0.02	17.9 0.6	43.5 0.3	0.27 0.04	0.19 0.00	–	–	–	101.1	0.81
Pl-core	7	46.7 0.3	–	33.0 0.3	–	0.46 0.03	0.10 0.01	–	17.4 0.2	0.02 0.00	1.60 0.2	–	99.3	0.86
Pl-core	1	48.0	–	33.7	–	0.55	0.11	–	16.8	0.03	2.12	–	101.4	0.81
Sp	1	0.02	1.73	21.6	26.5	24.1	8.37	0.31	0.02	–	–	18.8	101.5	
Sp	1	nd	11.6	2.90	12.2	37.0	3.48	0.39	0.06	–	–	33.4	101.1	
Sp	1	nd	18.2	1.66	0.17	43.3	2.69	0.50	0.23	–	–	33.2	100.0	
1471 M-A North group														
Ol-core	4	39.4 0.1	0.02 0.02	0.02 0	0.04 0.02	16.9 0.2	43.7 0.3	0.23 0.04	0.19 0.01	–	–	–	100.5	0.82
Ol-rim	1	37.5	0.02	0.04	0.08	27.09	34.81	0.39	0.3	–	–	–	100.2	0.70
Pl-core	5	47.0 0.4	–	33.82 0.65	–	0.50 0.05	0.12 0.02	–	17.38 0.36	0.03 0.01	1.72 0.2	–	100.6	0.85
Pl-rim	1	56.0	–	26.69	–	0.98	0.11	–	10.31	0.29	5.77	–	100.1	0.50

[a] Spinel: Fe_2O_3, FeO and total are based on 3 cation, 4 oxygen stoichiometry
[b] Two sigma deviation based on replicate analyses

Table 4 Run conditions, observed phases and their proportions. Proportions of phases determined by mass balance against the bulk composition 1471 M-B

Exp. #	T (C°)	Dur (h)	Phases Present	Phase Proportions	Σr^2
15	1075	10	gl, ol	1:tr	0.2
12	1050	18	gl, ol, pl, Cr-sp	0.96:0.02:0.02:tr	0.2
14	1045	20	gl, ol, pl, Cr-sp	0.89:0.04:0.06:tr	0.5
13	1035	24	gl, ol, pl, Cr-sp, aug	0.83:0.05:0.10:tr:0.02	0.6
2	1015	38	gl, ol, pl, aug	0.63:0.08:0.23:0.06	0.2
1	1000	36	gl, ol, pl, aug, mt	0.56:0.07:0.26:0.10:0.02	0.01
8	985	23	gl, ol, pl, aug, mt	0.53:0.08:0.28:0.10:0.01	0.03

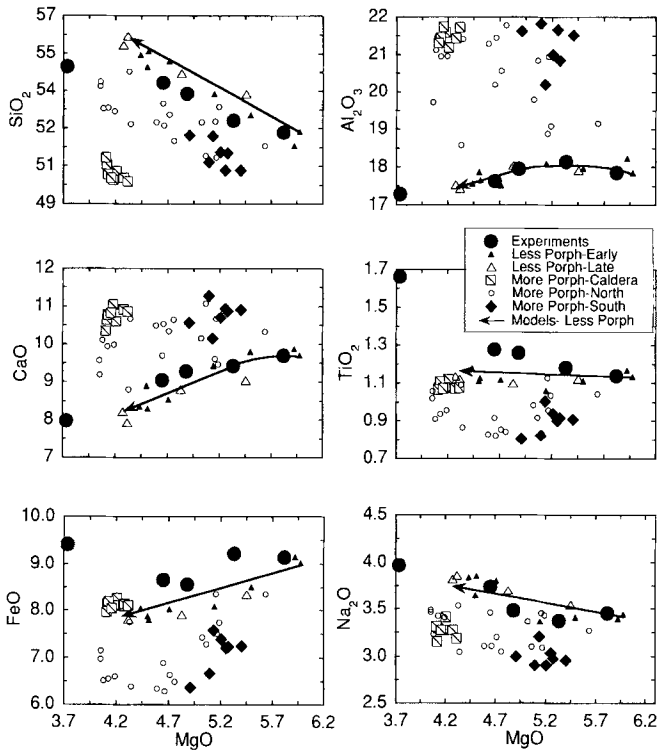

Fig. 2 MgO variation diagrams of major oxides for the lava samples of the Lake Basalt, experimental glasses and models of the less porphyritic lava samples. All values are in wt%. Data for the lava samples (Table 1) and the experimental glasses (Table 5) are normalized to 100%, volatile free. *Arrows* show compositional variation of the less porphyritic Lake Basalt models from Table 7, *arrow-tails* begin at 1471M-B. Two-sigma error bars for experimental glasses are smaller than their symbol. The two lowest temperature experiments are not plotted because their MgO contents are significantly lower than that of the Lake Basalt

2 kbar H_2O-saturated, Ni-NiO buffered basaltic liquids. Using this ratio to calculate the Fe^{2+} in our experiments and recalculating our exchange K_Ds gives an average value of 0.33. This is similar to the average value of 0.34 determined for the 1 kbar, H_2O-saturated experiments of Sisson and Grove (1993b) and within the range of K_Ds (0.26–0.36) determined by Roeder and Emslie (1970) for dry basaltic liquids.

Plagioclase

Phenocrysts generally grew as equant, homogeneous laths. Plagioclase present in the starting composition did not completely re-equilibrate in the two lowest temperature experiments but grew homogeneous reaction rims (>10 μm) that were analyzed. The Ca/Na exchange K_D for plagioclase [$K_D = (Ca_{pl}/Na_{pl})/(Ca_{liq}/Na_{liq})$] in the experiments ranged from 2.5 to 4.4 with an average value of 3.1 and was inversely correlated with temperature. This is similar to the average value of 3.3 determined for the 1 kbar, H_2O-saturated experiments of Sisson and Grove (1993b).

Spinel

Oxide phases are either Cr-sp or titanomagnetite, similar in composition to those present in the lavas. Spinel crystals are on the order of 2–3 μm in size, making quantitative analysis difficult. Cr-sp is present in experiments from 1050 to 1035°C, but was only large enough for quantitative analysis in the 1035°C experiment where a single large equant Cr-sp was analyzed. Spinel in the lower temperature experiments (run #s 1 and 8) is titanomagnetite. The loss of Cr-sp from the liquidus in the experiments concurs with the resorbed habit of Cr-sp surrounded by groundmass in the lavas.

High-calcium pyroxene

Cpx is not present as a phenocryst phase in 1471M-B and where present in the experiments grew from liquid. Assuming all Fe is FeO, the Fe/Mg exchange K_D ranged from 0.20 to 0.25 with an average value of 0.21 ± 0.02. This is similar to the average value of 0.22 determined for the 1 kbar, H_2O-saturated experiments of Sisson and Grove (1993b) as well as in the 1 atm (0.101 MPa) anhydrous experiments of Grove and Bryan (1983).

Discussion

Models of low-MgO HAB and BA genesis

The petrologic complexity of low-MgO HABs and BAs indicate that a variety of processes led to their origin. Low-MgO HABs and BAs often have very high plagioclase phenocryst contents, some in excess of 50 modal%, which can be correlated with bulk rock Al_2O_3 (Ewart 1982). The phenocrysts commonly have disequilibrium

Table 5 Experimental phase compositions (wt%) determined by electron microprobe (*Pts* number of analyses, * phase detected but too small for quantitative analysis, *nd* not detected, – not determined)

Exp. #	Phase	Pts	SiO_2	TiO_2	Al_2O_3	Cr_2O_3	FeO	MgO	MnO	CaO	K_2O	Na_2O	P_2O_5	Fe_2O_3	Total
15	gl[a]	11	51.8 (3)[b]	1.08 (4)	17.8 (2)	0.04 (3)	9.1 (2)	5.80 (4)	0.18 (5)	9.7 (1)	0.51 (3)	3.8 (1)	0.23 (3)	–	94.55
	ol	4	38.7 (3)	0.00 (1)	0.06 (1)	0.05 (1)	18.9 (2)	41.7 (1)	0.30 (3)	0.29 (3)	–	–	–	–	99.7
12	gl	15	52.3 (2)	1.12 (4)	18.1 (1)	0.04 (3)	9.2 (1)	5.31 (7)	0.14 (3)	9.4 (1)	0.48 (2)	3.7 (1)	0.24 (3)	–	96.19
	ol	7	38.6 (3)	0.03 (7)	0.07 (5)	nd	19.5 (3)	41.4 (3)	0.27 (3)	0.32 (3)	–	–	–	–	99.9
	pl	4	46.6 (5)	–	33.3 (4)	–	0.76 (5)	0.16 (5)	–	17.4 (3)	0.03 (1)	1.6 (2)	–	–	99.8
	Cr-sp[c]	*													
14	gl	11	53.5 (4)	1.19 (3)	17.9 (1)	0.04 (3)	8.5 (2)	4.86 (4)	0.18 (3)	9.2 (1)	0.54 (2)	3.8 (2)	0.24 (3)	–	95.46
	ol	5	38.6 (4)	0.11 (1)	0.09 (3)	0.04 (0)	20.3 (0)	40.1 (4)	0.35 (5)	0.33 (2)	–	–	–	–	99.6
	pl	4	47.9 (7)	–	32.8 (9)	–	0.8 (2)	0.2 (2)	–	16.7 (6)	0.03 (2)	2.0 (3)	–	–	100.3
	Cr-sp	*													
13	gl	11	53.9 (2)	1.21 (3)	17.6 (1)	nd	8.6 (1)	4.63 (3)	0.08 (4)	9.0 (1)	0.60 (2)	4.1 (1)	0.22 (2)	–	94.97
	ol	5	38.1 (5)	0.05 (1)	0.07 (3)	0.04 (1)	21.7 (6)	39.5 (7)	0.37 (2)	0.29 (2)	–	–	–	–	100.2
	pl	8	48.2 (8)	–	31.8 (7)	–	0.8 (2)	0.2 (1)	–	16.0 (6)	0.00 (1)	2.3 (3)	–	–	99.3
	aug	5	51 (1)	0.7 (1)	3.5 (6)	0.4 (2)	7 (1)	15.6 (4)	0.14 (3)	21.3 (5)	–	0.3 (1)	–	–	99.9
	Cr-sp	1	0	3.57	14.3	25.4	23.8	8.05	0.46	0.47	–	–	–	23.7	99.8
2	gl	10	54.6 (3)	1.58 (6)	17.2 (7)	0.05 (3)	9.4 (3)	3.7 (2)	0.19 (4)	7.9 (2)	0.72 (4)	4.4 (1)	0.29 (2)	–	95.57
	ol	6	37.2 (5)	0.03 (2)	0.06 (1)	0.02 (2)	25.7 (2)	36.1 (6)	0.43 (4)	0.32 (1)	–	–	–	–	99.3
	pl	8	50.8 (4)	–	30.3 (7)	–	0.85 (7)	0.22 (7)	–	14.5 (4)	0.08 (1)	3.2 (3)	–	–	100.0
	aug	12	51.6 (5)	0.82 (9)	3.0 (6)	0.29 (7)	7.8 (3)	15.3 (4)	0.20 (4)	21.10 (3)	–	0.31 (9)	–	–	99.8
1	gl	15	56.0 (3)	1.58 (5)	17.1 (3)	nd	8.9 (2)	3.3 (1)	0.15 (3)	7.3 (2)	0.80 (3)	4.6 (2)	0.28 (2)	–	95.97
	ol	12	36.9 (3)	0.06 (4)	0.06 (2)	nd	27.2 (4)	35.3 (4)	0.45 (4)	0.29 (3)	–	–	0.02 (1)	–	99.8
	pl	4	51.5 (7)	–	30.8 (4)	–	0.8 (1)	0.14 (4)	–	14.0 (4)	0.08 (2)	3.4 (3)	–	–	100.7
	aug	9	51.4 (5)	0.84 (9)	3.4 (5)	0.23 (8)	8.3 (6)	15.0 (5)	0.21 (7)	20.9 (7)	–	0.28 (6)	–	–	100.1
	mt	*													
8	gl	14	55.9 (3)	1.64 (4)	17.1 (2)	0.05 (3)	8.9 (1)	3.12 (7)	0.20 (3)	7.0 (1)	0.87 (3)	4.9 (1)	0.32 (3)	–	95.40
	ol	15	36.6 (3)	0.04 (5)	0.1 (1)	0.07 (1)	28.9 (4)	33.3 (5)	0.46 (4)	0.34 (4)	–	–	–	–	99.4
	pl	9	50.7 (7)	–	30.2 (8)	–	0.83 (6)	0.15 (4)	–	14.1 (6)	0.08 (3)	3.4 (3)	–	–	99.5
	aug	10	50.8 (6)	0.9 (1)	3.1 (3)	0.17 (5)	0.9 (7)	15.2 (5)	0.21 (6)	20 (1)	–	0.33 (5)	–	–	99.7
	mt	5	0.1 (1)	15.6 (4)	4.9 (1)	2.9 (2)	38.7 (3)	4.3 (1)	0.43 (1)	0.4 (1)	–	–	–	31.6	99.0

[a] Glass analyses are normalized to 100% on a volatile-free basis; the original total is reported in Total column

[b] Values in parentheses are the two sigma deviations based on replicate analyses

[c] For spinel analyses all Fe was originally determined as FeO. Reported Fe_2O_3, FeO and Total for spinels are recalculations based on a stoichiometry of 3 cations and 4 oxygens

textures and variable compositions, indicating crystallization under a variety of conditions. These observations and other geochemical evidence led Crawford et al. (1987) to conclude that HABs with >18 wt% Al_2O_3 form by plagioclase accumulation. They argued that liquids produced by differentiation contain <17.5 wt% Al_2O_3 and are produced through olivine- and clinopyroxene-controlled differentiation of less aluminous mantle melts. Many other studies (e.g. Kay et al. 1982; Gust and Perfit 1987) conclude that the compositional variation in HABs is consistent with an origin by differentiation. Nevertheless, anhydrous experimental studies have been unable to produce typical low-MgO HAB and BAs by crystallization of either high- or low-Al_2O_3 parent compositions at any pressure (Gust and Perfit 1987; Bartels et al. 1991; Draper and Johnston 1992). Hydrous experimental studies, on the other hand, have shown that differentiation with dissolved water contents of 4 to 6 wt% can produce liquids with compositions similar to typical low-MgO HABs and BAs (Sisson and Grove 1993b; Gaetani et al. 1993). Water contents of this magnitude have been observed in melt inclusions from arc environments (Anderson 1979; Sisson and Layne 1993). Sisson and Grove (1993b) proposed that high dissolved water contents produce the high phenocryst contents of low-MgO HABs and BAs; as rising magmas degas, the corresponding rise in liquidus temperature and shift of phase boundaries would cause plagioclase crystallization.

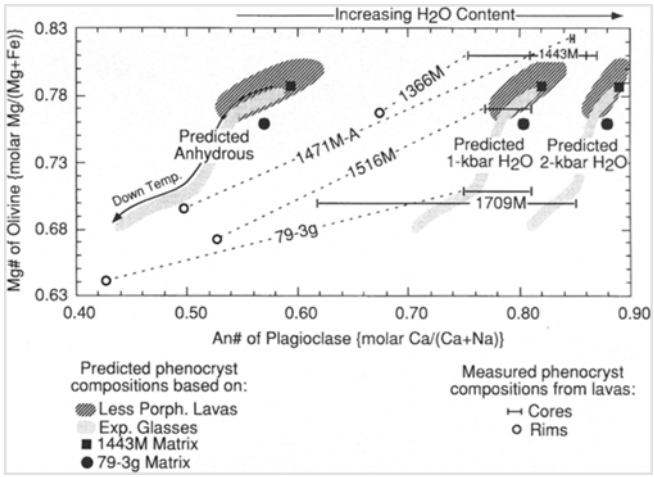

Fig. 3 Comparison of measured phenocryst compositions of lavas of the Lake Basalt with those predicted as a function of magmatic water content, Mg# of olivine against An# of plagioclase. *Dashed lines* connect cores to measured phenocryst rim compositions. Predicted phenocryst compositions are based on the less porphyritic lava samples, the experimental glasses and the matrix separates of the more porphyritic lava samples (Table 9). Plagioclase Ca/Na exchange K_D varies from 1 ("Predicted Anhydrous") to 3.1 ("Predicted 1 kbar H_2O") to 5.5 ("Predicted 2 kbar H_2O"). Fe/Mg exchange K_D for olivine was held constant at 0.29. Rim compositions were not analyzed on 1443 M or 1709M, but were present in each sample

Magmatic H_2O contents of lavas of the Lake Basalt

Though magmas can have significant dissolved H_2O contents at crustal pressures, they undergo rapid devolatilization during eruption. Unaltered lavas generally have less than 0.1 wt% dissolved H_2O. Pre-eruptive H_2O contents can be estimated based on plagioclase phenocryst composition since melt H_2O content is positively correlated with the anorthite content of coexisting plagioclase (e.g. Yoder 1969; Arculus and Wills 1980; Housh and Luhr 1991). The plagioclase-liquid Ca/Na exchange K_D has a value of ~1 under anhydrous conditions, increasing to ~3.1 at dissolved water contents of 4 wt% (this study) and further increasing to ~5.5 at water contents of 6 wt% (Sisson and Grove 1993a). These values were used to calculate the plagioclase compositions that would coexist with the less porphyritic lavas and the experimental glasses (Fig. 3). Calculations using the more porphyritic lavas as melts yield similar results. The anorthite contents of the plagioclase phenocryst cores of the more and less porphyritic lavas are similar to those predicted to coexist with melts containing 4 to 6 wt% dissolved H_2O (1-to 2-kbar H_2O saturated conditions). These are the same conditions predicted by Sisson and Grove (1993b) for formation of low-MgO HABs and BAs by differentiation. The plagioclase phenocryst rim compositions approach those predicted for dry conditions and indicate that rim growth continued after degassing, probably during eruption or shallow level storage. Olivine core compositions of 79–3g and 1709M have Mg#s much lower than would be in equilibrium with the matrix separates or the less porphyritic lavas, but are similar to the lowest temperature experimental liquids. Olivine cores of 1471M-A, 1366M and 1443M indicate crystallization in magmas with higher Mg#s than the most primitive sampled lava.

The liquid line of descent followed by a magma will also vary as a function of dissolved H_2O content. Figures 4a and 4b show the anhydrous and hydrous crystallization paths for 1471M-B, the most primitive less porphyritic lava and experimental starting composition. The 1 kbar anhydrous ol-cpx-pl crystallization boundary has been predicted using the equations of Yang et al. (unpublished work, 1993) that parameterize 175 ol-cpx-pl saturated basaltic liquids in the 0.101 MPa to 10 kbar range from the experimental literature. The anhydrous boundary reduces to a point in the Ol-Pl-Cpx projection (Fig. 4a) since it is nearly perpendicular to the ol-cpx-pl plane. In the Cpx-Pl-Qtz (Fig. 4b) projection the boundary projects as a line. 1471M-B projects in the anhydrous plagioclase liquidus phase volume. If 1471M-B liquid underwent anhydrous crystallization, residual liquids would move towards ol-cpx-pl saturation by crystallizing plagioclase until intersection with the ol-pl cotectic (point 1 in Fig. 4a). None of the lavas plot along the anhydrous path in either projection.

The addition of water changes the direction of crystallization and generates a path that parallels the shape of the field defined by the less porphyritic lavas. Hydrous differentiation, as initially determined by Yoder (1965)

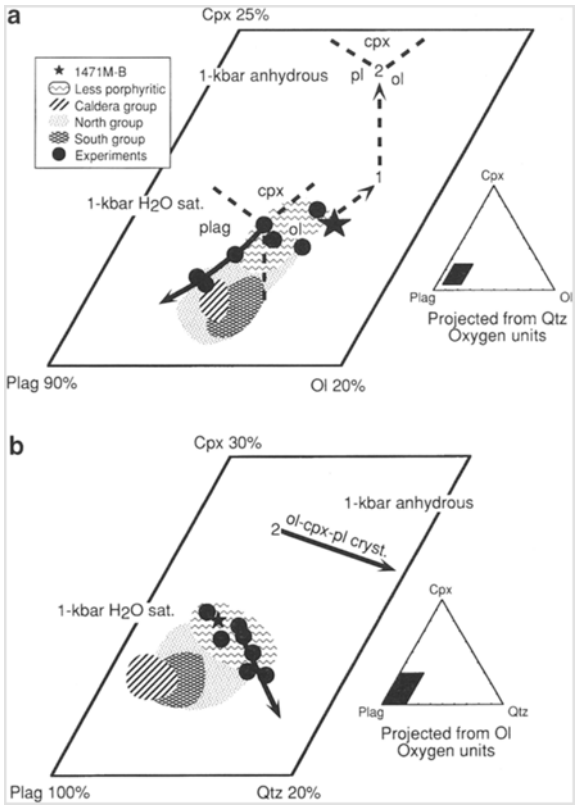

Fig. 4a, b Normative projections using the equations of Grove (1993). *Arrows* point in down temperature directions. **a** Pl-Cpx-Ol projection (critical plane of silica undersaturation). *Solid curve* represents 1 kbar water-saturated ol-cpx-pl crystallization boundary as determined by the experiments in this study. *Dashed lines* schematically show phase boundaries and 1 kbar anhydrous crystallization path. *Point 1* shows the beginning of ol-pl cosaturation during 1 kbar anhydrous crystallization, *point 2* shows ol-pl-cpx saturation as predicted by the equations of Yang et al. (unpublished, 1993). **b** Pl-Cpx-Qtz projection. *Solid curves* represent 1 kbar ol-cpx-pl boundaries

in the system diopside-anorthite, expands the diopside primary phase volume at the expense of anorthite. The hydrous ol-cpx-pl boundary is redirected in the Ol-Cpx-Pl projection to trend towards the Pl apex. For hydrous crystallization of 1471M-B, olivine becomes the liquidus phase. A small amount of olivine crystallization, followed by Cr-sp and pl, leads to ol-cpx-pl multiple saturation. The less porphyritic lava samples plot near the 1 kbar H_2O saturated boundaries in both projections, while the more porphyritic lavas are displaced towards the plagioclase apex in the Cpx-Pl-Qtz projection (Fig. 4b).

Petrogenesis of the less porphyritic lavas

The less porphyritic lavas show major element compositional variation broadly similar to the liquid line of descent followed by the experiments. However, CaO, FeO and TiO_2 contents of the lavas are lower while SiO_2 contents are higher than the experimental liquids at corresponding MgO contents (Fig. 2). Trace element concentrations in the experimental liquids were calculated for a simple fractional crystallization model (Table 6, Fig. 5). The trace element abundances of the calculated fractionation path are not similar to the less porphyritic lava samples for several key elements. K_2O, Ba and Rb abundances are progressively enriched in the less porphyritic lava samples relative to the calculated fractionation path. Although the variations in the major element concentrations of the less porphyritic lavas resemble those of the experiments, fractionation of the most commonly observed phenocrysts (ol and pl) cannot be solely responsible for the observed chemical variations. We conclude that open system processes operated in the magma system. Many studies (Eichelberger 1975; Anderson 1976; Grove et al. 1988; Baker et al. 1991; Donnelly-Nolan et al. 1991) have concluded that magmatic systems at MLV

Table 6 Calculated trace element abundances of liquids following the experimental crystallization sequence (ppm)

Phase	La	Ce	Nd	Sm	Eu	Yb	Lu	Hf	Ta	Th	Rb	Sr	Zr	Nb	Ba
Partition coefficients[a]															
Olivine	0.008	0.008	0.006	0.005	0.005	0.009	0.009	0.004	0.010	0.01	0.010	0.010	0.005	0.010	0.010
Plagioclase	0.302	0.221	0.149	0.102	1.214	0.041	0.039	0.015	0.025	0.010	0.070	1.800	0.013	0.025	0.160
Augite	0.105	0.125	0.287	0.477	0.562	0.601	0.560	0.121	0.300	0.010	0.020	0.080	0.131	0.300	0.020
Bulk distribution coefficients for experimental liquids[b]															
Experiment F															
12 0.96	0.155	0.115	0.077	0.054	0.610	0.025	0.024	0.009	0.018	0.010	0.040	0.905	0.009	0.018	0.085
14 0.89	0.205	0.151	0.102	0.070	0.815	0.030	0.029	0.011	0.020	0.010	0.050	1.209	0.010	0.020	0.111
13 0.83	0.202	0.162	0.166	0.193	0.850	0.193	0.180	0.043	0.100	0.010	0.047	1.050	0.045	0.100	0.098
Calculated abundances for 1471 M-B liquids[c]															
12	8.18	19.1	10.9	3.42	1.19	2.87	0.41	2.47	0.21	1.03	16.1	488	109	5.36	214
14	8.68	20.3	11.7	3.67	1.21	3.09	0.45	2.66	0.23	1.11	17.3	481	117	5.78	229
13	9.18	21.6	12.4	3.88	1.22	3.27	0.47	2.84	0.24	1.19	18.5	479	125	6.15	244

[a] Data sources for partition coefficients: Sr, Rb, Ba, Th, Ta and Nb from Gill (1981), REE, Hf and Zr from Fujimaki et al. (1984)
[b] Bulk partition coefficients determined using experimental phase proportions from Table 4
[c] Elemental abundances for 1471 M-B from Table 1. Fractionation calculations for differentiated liquids calculated using equations of Allègre and Minster (1978)

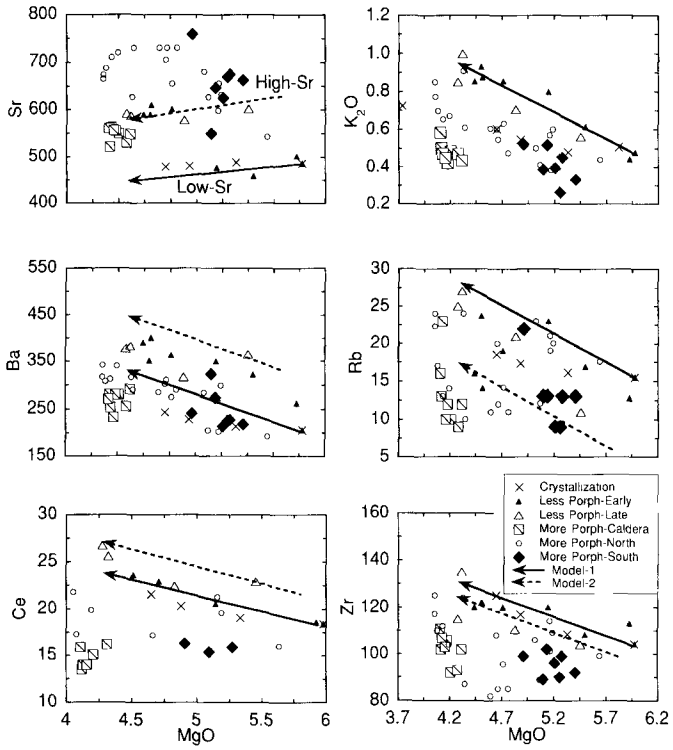

Fig. 5 Selected trace element and K_2O abundances plotted against MgO for lavas and models. K_2O and MgO in wt%. Sr, Rb, Ba, Ce and Yb in ppm. Crystallization points (*crosses*) are from Table 6. *Arrows* are FARM model compositions from Table 8 that employ fractional crystallization, assimilation and mixing. *Tails of Model-1 arrows* begin at 1471M-B, *tails of Model-2 arrows* begin at calculated 1281M pre-assimilation discussed in text

experienced complex, open-system processes including assimilation and magma mixing. The resorbed textures and common reverse compositional zonation of plagioclase phenocrysts in the lavas of the Lake Basalt led Anderson (1941) and Gerlach and Grove (1982) to conclude that these lavas formed by open system processes. Baker et al. (1991) recognized such complexities as the FARM process (Fractionation, Assimilation, Replenishment and Mixing) for the Giant Crater lava field.

Major element FARM models

The major element compositions of all of the less porphyritic lava samples were modeled using a FARM model (Table 7, Fig. 2) following the method of Baker et al. (1991). A unit of parent liquid differentiates and supplies heat to melt granitic crust. The magma system is subsequently replenished with undifferentiated parent liquid which mixes with the melted crust and differentiated liquid. The glass compositions from experiments 13 and 14 were chosen as the differentiated liquids. These experiments contained little to no cpx (Table 4) which is consistent with the lack of cpx in the lavas. Using lower temperature experiments did not improve the fit of any models. A partially melted granitic xenolith from the Lake Basalt, (561M, Grove et al. 1988) was chosen as the assimilant composition. There are a variety of other granitic inclusions found at MLV (Grove et al. 1988), but varying the composition of granitic assimilant did not result in significantly better fits to the lava compositions. Sample 1471M-B, the most primitive less porphyritic lava sample, was used for the replenishing liquid. Proportions of each of the components were determined by multiple linear regression for each less porphyritic lava composition. Complete FARM models generally result in a significantly better fit to the data set than assimilation and fractional crystallization (AFC) models. Two (1344M and 313M) lavas can be equally well reproduced using only AFC and one (1444M) can be reproduced using only FRM. Major element contents of most samples were reproduced to better than 2% relative and minor oxides (TiO_2 and K_2O) were well reproduced for most samples.

Trace element FARM models

The proportions of FARM components from the major element regressions of Table 7 were used in trace element modeling of the less porphyritic lavas (Table 8, Fig. 5). The Sr abundances of the less porphyritic lavas form two distinct trends that have similar slopes, but are offset in concentration by approximately 25% (Fig. 5). The low-Sr trend was well reproduced by the FARM model used for the major elements, which uses 1471M-B as the parent for the fractionating and replenishing liquid (denoted Model-1 in Table 8 and Fig. 5). A second model was developed to reproduce the high-Sr trend. Model-2 uses the most primitive lava of the late less porphyritic group, 1281M, for the fractionating and replenishing liquid. It has undergone some assimilation of granitic crust based on the FARM model calculation for major elements. It was corrected to its pre-assimilation trace element abundance levels based on the proportions from the major element model (Table 7), 6 wt% of 561M was subtracted from it. Recalculating the major element FARM models using the 1281M-based parent reproduces some of the minor element abundances better than Model-1, but does not make a significant difference for the other major elements. Most of the variations in abundances shown by the less porphyritic lavas fall within the trends defined by Model-1 and -2. Model-1 abundances define the lower limit of variation in Sr, Ba and Nd and the upper limit of variation in the Rb and Zr variation diagrams. Model-2 forms complementary trends that define the upper limit of variation on the Sr, Ba and Nd and the lower limit in the Rb and Zr variation diagrams.

The low-Sr trend contains early less porphyritic lavas and is similar in concentration and slope to Model-1. The high-Sr trend contains two of the early and all of the late less porphyritic samples and is overlapped in concentration and slope by Model-2. In other words, using the most primitive early lava (1471M-B) as a parent generally reproduces the early lavas (Model-1), while using the most primitive late lava (1281M) as a parent repro-

Table 7 Major element FARM models for less porphyritic lavas[a]
Model=Differentiated liquid (from experiments)[b]+Primitive liquid (1471 M-B)+Granitic assimilant (561 M)[c]

Sample	Results									Components			
	SiO_2	Al_2O_3	FeO	MgO	CaO	Na_2O	K_2O	TiO_2	Σr^2	Diff. lq wt%	Diff. lq wt%	1471 M-B	wt% 561 M
Less Porphyritic – Early													
1246 M Composition	55.3	17.6	8.05	4.73	8.57	3.82	0.86	1.12					
Model	55.3	17.5	8.14	4.73	8.58	3.68	0.87	1.14	0.04	Exp 13	0.53	0.36	0.11
1344 M Composition	55.0	17.9	7.90	4.52	8.93	3.66	0.93	1.11					
Model	55.0	17.8	8.11	4.59	8.77	3.53	0.77	1.20	0.1	Exp 14	0.92	–	0.07
1444 M Composition	52.9	18.0	8.53	5.52	9.83	3.42	0.62	1.11					
Model	52.9	17.9	8.85	5.52	9.54	3.47	0.51	1.19	0.2	Exp 14	0.44	0.56	–
1762 M Composition	53.9	18.2	8.11	5.16	9.46	3.38	0.80	1.07					
Model	54.0	17.9	8.56	5.11	9.25	3.50	0.61	1.20	0.4	Exp 14	0.68	0.29	0.03
1778 M Composition	55.6	17.6	8.07	4.45	8.39	3.85	0.86	1.18					
Model	55.6	17.5	8.10	4.44	8.48	3.75	0.87	1.18	0.04	Exp 13	0.78	0.12	0.10
1784 M Composition	55.7	17.7	7.83	4.53	8.33	3.87	0.88	1.13					
Model	55.7	17.6	7.84	4.52	8.45	3.56	0.92	1.13	0.1	Exp 14	0.72	0.15	0.13
Less Porphyritic – Late													
313 M Composition	55.9	17.6	8.09	4.29	8.24	3.83	0.85	1.14					
Model	55.9	17.5	8.06	4.28	8.40	3.79	0.88	1.20	0.05	Exp 13	0.90	–	0.10
1281 M Composition	53.9	18.0	8.37	5.48	9.07	3.56	0.56	1.13					
Model	53.9	17.8	8.54	5.41	9.17	3.51	0.69	1.13	0.1	Exp 14	0.25	0.69	0.06
1343 M Composition	54.7	18.1	7.93	4.85	8.83	3.71	0.71	1.10					
Model	54.8	17.8	8.23	4.78	8.88	3.53	0.74	1.18	0.2	Exp 14	0.77	0.16	0.07
1668 M Composition	56.4	17.5	7.84	4.34	7.96	3.88	1.00	1.13					
Model	56.4	17.4	7.79	4.30	8.16	3.76	1.01	1.13	0.08	Exp 13	0.68	0.17	0.15

[a] FARM models are calculated by least squares multiple linear regression of the differentiated liquid, primitive liquid, and assimilant against the bulk composition of each sample. All compositions normalized to 100% without Cr_2O_3, MnO and P_2O_5

[b] Differentiated liquids are the experimental glasses (Table 5) with TiO_2 and Na_2O concentrations corrected for bias as discussed in text

[c] Granitic assimilant is 561 M reported by Grove et al. (1988)

duces some of the early and all of the late lavas (Model-2).

Petrogenesis of the more porphyritic lavas

Moderately porphyritic lavas

The North group lavas with Al_2O_3 < or = 19.2 wt% (1471M-A, 1669M, 1670M and 1725M) have the lowest phenocryst contents of the porphyritic samples. With the exception of their higher Al_2O_3 contents, they are chemically similar to the less porphyritic lavas (Figs. 2, 5, 6) and form trends consistent with either an accumulation or a differentiation origin. 1471M-A has approximately 7 modal% phenocrysts and was collected from the same outcrop as less porphyritic lava 1471M-B, which is nearly aphyric. Addition of 7 wt% plagioclase to 1471M-B can nearly produce the bulk composition of 1471M-A. The experiments of Sisson and Grove (1993a) show that the plagioclase phase volume shrinks with increasing dissolved H_2O, resulting in increased liquid Al_2O_3 contents during differentiation. Ol-pl-cpx-H_2O saturated liquids at 2 kbar contain approximately 20 wt% Al_2O_3. The moderately porphyritic North group lavas could represent liquids that differentiated at 2-kbar with dissolved water contents of up to 6 wt%, which led to their higher Al_2O_3 contents. Their higher phenocryst contents relative to the less porphyritic lavas could reflect in situ phenocryst growth during degassing of higher water content magma that occurred during decompression and eruption.

Highly porphyritic lavas

The majority of the more porphyritic lavas have >20 wt% Al_2O_3 and >18 modal% phenocrysts. Liquids with Al_2O_3 contents of this magnitude might be produced by H_2O-saturated differentiation at pressures >2 kbar, however the plagioclase phenocrysts found in these lavas have anorthite contents consistent with crystallization under H_2O-saturated conditions of only 1 or 2 kbar (Fig. 3). Furthermore, these porphyritic lavas plot away from the differentiation trend and lie along a plagioclase addition line (Fig. 4b). The major oxides and trace elements incompatible in ol, cpx and pl (Na_2O, TiO_2 and Ba, K_2O, Ce, Zr and Rb) are depleted in the more porphyritic South group and most of the North group lavas relative to the less porphyritic lavas (Figs. 2, 5). Therefore these more porphyritic lavas cannot be related to the less porphyritic lavas through differentiation.

Variations in the Sr/Zr ratio also indicate that the most porphyritic lavas are not related to each other or the less porphyritic lavas through differentiation. The Sr/Zr ratios (Fig. 6) of the more porphyritic lavas are highly

Table 8 Trace element FARM models for less porphyritic lavas (ppm)[a]

Sample	La	Ce	Nd	Sm	Eu	Yb	Lu	Hf	Ta	Th	Rb	Sr	Zr	Nb	Ba
Less porphyritic – Early															
1246 M	11.1	22.9	13.0	3.54	1.20	1.90	0.28	2.30	0.24	1.70	19.0	601	120	6.00	363
Model-1[b]	10.1	22.6	12.4	3.70	1.17	2.93	0.43	2.90	0.31	2.15	25.3	455	124	5.66	299
Model-2[c]	12.5	25.8	16.6	4.03	1.26	2.19	0.35	2.54	0.25	1.71	15.4	579	118	2.32	4.21
1344 M	10.8	23.3	13.0	3.47	1.24	1.97	0.29	2.40	0.25	1.65	23.7	590	122	3.62	351
1	9.7	21.9	12.2	3.70	1.18	2.99	0.43	2.83	0.29	1.82	22.8	461	122	5.71	277
2	12.1	25.2	16.5	4.04	1.28	2.22	0.35	2.45	0.22	1.37	12.5	590	116	2.23	404
1444 M	–	–	–	–	–	–	–	–	–	–	16.9	459	108	5.54	322
1	8.2	19.2	11.0	3.45	1.18	2.90	0.42	2.50	0.22	1.04	16.3	484	110	5.42	216
2	10.8	22.6	15.4	3.81	1.29	2.12	0.34	2.12	0.15	0.58	5.8	623	104	1.89	345
1762 M	10.0	20.6	11.3	3.52	1.19	2.11	0.33	2.50	<0.3	1.89	23.0	477	120	8.00	350
1	8.9	20.4	11.6	3.58	1.19	2.96	0.43	2.64	0.24	1.35	18.9	476	115	5.58	241
2	11.4	23.8	16.0	3.93	1.29	2.17	0.35	2.26	0.18	0.89	8.4	612	109	2.04	370
1778 M	–	–	–	–	–	–	–	–	–	–	16.0	590	120	–	390
1	10.3	23.2	12.8	3.83	1.18	3.06	0.45	2.99	0.31	2.10	25.3	456	128	5.91	301
2	12.8	26.5	17.2	4.18	1.28	2.28	0.37	2.61	0.25	1.63	14.8	581	122	2.38	430
1784 M	10.8	23.6	13.2	3.62	1.23	1.96	0.28	2.62	0.34	1.90	14.0	610	122	–	400
1	10.3	22.8	12.5	3.67	1.16	2.87	0.42	2.91	0.32	2.34	26.7	449	123	5.57	310
2	12.6	25.8	16.4	3.99	1.25	2.16	0.35	2.57	0.27	1.92	17.1	569	118	2.36	427
Less porphyritic – Late															
313 M	10.8	26.7	14.8	3.55	1.27	1.77	0.32	2.58	0.24	1.73	25.0	592	115	5.00	377
1	10.5	23.6	13.0	3.91	1.19	3.12	0.45	3.05	0.32	2.13	25.7	455	131	6.04	307
2	13.0	27.0	17.5	4.26	1.28	2.33	0.37	2.66	0.25	1.66	15.0	579	125	2.42	438
1281 M	11.1	22.9	15.0	3.66	1.25	2.00	0.32	2.20	0.20	1.20	11.0	602	104	2.00	365
1	9.0	20.4	11.4	3.45	1.17	2.79	0.40	2.61	0.26	1.65	20.8	470	113	5.31	255
2	11.4	23.5	15.4	3.77	1.26	2.06	0.33	2.27	0.20	1.22	11.2	601	107	2.06	375
1343 M	10.5	22.4	13.5	3.40	1.21	1.80	0.26	2.34	0.24	1.55	21.0	578	110	6.31	317
1	9.5	21.5	12.0	3.64	1.18	2.95	0.43	2.77	0.28	1.76	22.2	464	119	5.62	270
2	11.9	24.8	16.3	3.98	1.28	2.18	0.35	2.40	0.22	1.31	12.0	593	114	2.18	396
1668 M	12.4	25.6	14.4	3.56	1.31	2.16	0.31	2.88	0.34	2.32	27.0	587	135	7.00	383
1	10.9	24.1	13.1	3.82	1.17	2.96	0.43	3.09	0.35	2.60	29.0	443	130	5.80	334
2	13.3	27.2	17.2	4.15	1.25	2.23	0.36	2.73	0.29	2.17	19.2	561	125	2.51	454

[a] Mixing models based on proportions calculated from the major element mass balances in Table 7. Elemental abundances for lavas from Table 1

[b] Model-1 uses 1471 M-B as parent composition for differentiated liquids (Table 6) and the primitive liquid recharge

[c] Model-2 uses the pre-assimilation corrected 1281 M as parent composition for differentiated liquids and the primitive liquid recharge

variable and enriched relative to the less porphyritic lavas, which form trends consistent with the FARM model. Olivine and cpx fractionation increases the residual liquid's Al_2O_3 content, but has little effect on its Sr/Zr ratio (partition coefficients in Table 6). Plagioclase crystallization would decrease the Sr/Zr ratio and retard any Al_2O_3 increases during crystallization so it was left out to maximize differentiation effects. Crystallization of ol and cpx defines nearly horizontal lines in Fig. 6. Twenty-four percent crystallization of 15% olivine and 85% clinopyroxene from 1471M-B only changes the Sr/Zr ratio from 4.67 to 4.72. The Al_2O_3 content of the liquid rises from 17.9 to 22 wt%, the lava maximum, but lowers the MgO content from 5.98 to 2.50, well below that observed in the lavas. MgO/Al_2O_3 ratio drops from 0.33 to 0.11. The other major element concentrations of the liquid are significantly different from those observed in the more porphyritic lavas. The South group and most of the North group lavas have $Sr/Zr > 6$, while all of the less porphyritic lavas have $Sr/Zr < 6$. Therefore, the Sr/Zr ratios of the most of the North and South group lavas are too high to be related to any of the less porphyritic lavas through crystallization. Production of the more porphyritic lavas by differentiation could have involved an unsampled parent with a high Sr/Zr ratio. However, the variability in the Sr/Zr ratio of the more porphyritic lavas at nearly constant MgO/Al_2O_3 ratio is difficult to explain by a differentiation process. We conclude that the more porphyritic North and South group lavas with >19.7 wt% Al_2O_3 are not related to each other or the less porphyritic lavas through a differentiation mechanism and are likely produced through a process of phenocryst accumulation at a pressure/depth similar to the one that generated the less and moderately porphyritic lavas. The accumulation model is also supported by the composition of the matrix separate of 1443M (Table 9), which is very similar to the less porphyritic lava compositions.

Accumulation constraints

To estimate the proportions and compositions of the entrained phenocrysts in the more porphyritic lavas, the bulk rock compositions of samples 1443M (South group)

Table 9 Mass balance models for the more porphyritic lavas (wt% normalized to 100 without P_2O_5 and MnO)

Sample	SiO_2	TiO_2	Al_2O_3	FeO*	MgO	CaO	K_2O	Na_2O	Total	Proportions[a]	Σr^2
79-3g	50.8	1.12	21.1	8.30	4.12	10.7	0.48	3.32	100.0		
Model	50.8	1.15	21.1	8.21	4.15	10.6	0.47	3.31	99.8		0.02
Matrix[b]	51.6	1.39	18.7	9.78	5.02	9.46	0.55	3.57	100.0	0.83	
High-An Pl[c]	47.9	0.00	33.0	0.74	0.01	16.1	0.07	2.12	100.0	0.17	
1443 M	51.3	0.92	20.9	7.26	5.30	10.9	0.45	2.99	100.0		
Model	51.3	0.94	21.0	7.32	5.28	10.8	0.40	2.83	99.8		0.05
Matrix	52.9	1.21	18.7	8.66	5.20	9.51	0.51	3.24	100.0	0.78	
Ol	38.9	0.00	0.03	17.8	43.1	0.19	0.00	0.00	100.0	0.03	
High-An Pl	47.0	0.00	33.2	0.46	0.10	17.5	0.02	1.61	100.0	0.19	

[a] Proportions calculated by least squares multiple linear regression
[b] Matrix is analyzed glass from melted matrix separates described in Experimental methods section
[c] Phenocryst compositions are from Table 3

and 79–3g (Caldera group) were mass balanced against their groundmass separates and phenocryst compositions (Table 9). All of the observed phenocryst phases with a complete range of plagioclase compositions were included in the mass balances, but only the most anorthite-rich plagioclase and some olivine was required to reproduce the bulk rocks. Olivine and spinel phenocrysts are much smaller in size than plagioclase phenocrysts and hence may not have been as effectively removed during matrix separation. More albitic plagioclase did not significantly improve the models of either sample.

Accumulation models

The mass balance proportions from Table 9 were used to model the effects of phenocryst accumulation on the Sr/Zr and MgO/Al_2O_3 ratios of various less porphyritic lavas (Fig. 6). Plagioclase accumulation increases the Sr/Zr ratio and decreases the MgO/Al_2O_3 ratio. The relatively minor amount of olivine accumulation has little effect on the Sr/Zr ratio, but somewhat counters the effect of plagioclase accumulation on the MgO/Al_2O_3 ratio. The models of plagioclase and olivine accumulation (Fig. 6) use the proportions estimated for phenocryst accumulation in 1443M of the South group. Three wt% olivine and 19 wt% plagioclase were added to the less porphyritic lavas with MgO contents near those of the 1443M matrix separate, 1281M of the high-Sr series and 1444M of the low-Sr series. Trace element abundances of accumulated phenocrysts are in equilibrium with a 1471M-B liquid composition from Table 6 that has an MgO content nearest to that of the matrix separate. The accumulation lines approximately define the field of South group lavas in Fig. 6. A model of plagioclase-only accumulation (Fig. 6) uses the proportions estimated for accumulation in sample 79–3 g of the Caldera group. It adds 18 wt% plagioclase (Table 9) to less porphyritic sample 1762M, which has a similar MgO content to the matrix separate of sample 79–3 g. The accumulation line ends right in the field of the Caldera group lavas, though based on other constraints it is not clear that the Caldera group is chemically related to the other lavas of the Lake

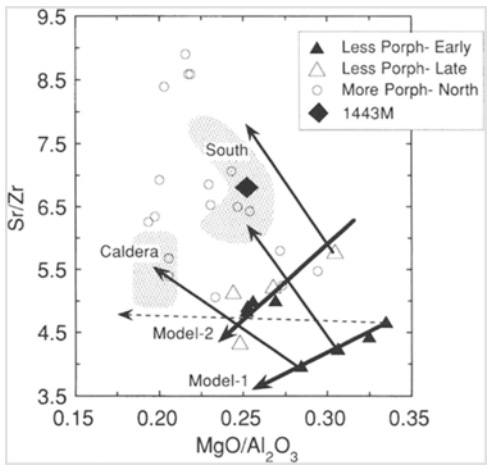

Fig. 6 Plagioclase compatible/incompatible vs incompatible/compatible element ratio plot to illustrate the relationship between more and less porphyritic lavas. Dashed arrow shows effect of ol+cpx crystallization on 1471M-B. *Thick solid arrows* represents FARM models. *Thin solid arrows* show the effect of pl±ol accumulation on less porphyritic lava compositions

Basalt. It is clear from Fig. 6 that pl and ol addition models can reproduce the entire spectrum of more porphyritic lavas from the less porphyritic lavas and we conclude that plagioclase accumulation is viable mechanism for more porphyritic lava formation.

Caldera group lavas

The lavas of the Caldera group differ from the more and less porphyritic lavas in having FeO and TiO_2 concentrations similar to the less porphyritic lavas (Fig. 2). This similarity might support a differentiation origin, but all of the incompatible element abundances of the Caldera group lavas are depleted with respect to the less porphyritic lavas and in this regard they resemble the other more porphyritic lavas (Fig. 5). Field constraints show that the Caldera group erupted before the other lavas of the Lake Basalt and from the E-W vent trend rather than the much larger NNW trend that vented the North and South groups. Therefore the Caldera group may sample a

different magmatic system of which a less porphyritic member is either not erupted or not exposed. The phenocryst textures and compositions found in the Caldera group are identical to the those of the North and South groups and likely formed by the same hydrous fractionation and plagioclase accumulation mechanisms.

Conclusions

We conclude that the lavas of the Lake basalt were formed by a combination of hydrous FARM differentiation and phenocryst accumulation. Plagioclase phenocrysts found in the lavas crystallized from magmas with dissolved H_2O contents of 4 to 6 wt%. The less porphyritic lavas formed by FARM differentiation with dissolved water contents of approximately 4 wt%, while the most porphyritic lavas formed by plagioclase crystal accumulation in these magmas. These conclusions combine the hydrous differentiation model of Sisson and Grove (1993b) with the plagioclase accumulation model of Crawford et al. (1987). Moderately porphyritic lavas fall in a crossover region where differentiation and accumulation cannot be uniquely constrained. Thus, liquids in the Lake Basalt magmatic system had at least 18.2 wt% Al_2O_3 and possibly up to 19.2 wt%, significantly higher than the limits proposed by Crawford et al. (1987), but slightly lower than the Al_2O_3 solubility limit determined by Sisson and Grove (1993a,b) for 1 to 2 kbar H_2O saturated liquids.

The magmatic system that produced these lavas preferentially segregated and concentrated plagioclase phenocrysts into the more porphyritic lavas. Brophy (1989) proposed that simultaneous crystallization and convection in magma chamber could cause such sorting. There is evidence of at least 1 km^3 sized magma chambers beneath MLV (Baker et al. 1991). A multiply recharged magma chamber is consistent with the FARM model we developed. The most differentiated liquids used in the FARM modeling crystallized approximately 10 wt% plagioclase. The most porphyritic lavas have almost twice that amount and hence there should twice as much less porphyritic than more porphyritic material, which is not supported by the mapped area. This unaccounted for less porphyritic component could be trapped at depth or simply buried beneath the more porphyritic lavas. Alternatively, the plagioclase phenocrysts could be related to the formation of andesites that are present in abundance in the older eruptive sequence at MLV. The differentiating liquids that produced these lavas may have remained hot enough to be entrained by the magmas of the Lake Basalt.

Acknowledgements A. Brandon, D.E. Champion, N. Chatterjee, F.A. Frey, G.A. Gaetani, A. Saal and E. Takazawa are thanked for helpful discussion and reading of earlier versions of the manuscript. H.J. Yang is thanked for the use of his equations for predicting the anhydrous phase boundaries. S.I. Recca and M.J. Jercinovic expertly maintained the MIT electron microprobe facility during the course of this study. The geo-artistic talents of E.B. Lougee created Fig. 1. The senior author wishes to thank T.W. Sisson for helpful direction early on in the project and two rounds of formal review. This paper also benefited from reviews by C. Bacon and anonymous reviewer. This work was supported by NSF grant # EAR-9204661 and EAR-9406177.

References

Albee AL, Ray L (1970) Correction factors for electron microprobe microanalysis of silicates, oxides, carbonates, phosphates and sulfates. Anal Chem 42: 1408–1418

Allègre CJ, Minster JF (1978) Quantitative models of trace element behavior in magmatic processes. Earth Planet Sci Lett 38: 1–25

Anderson AT (1976) Magma mixing: petrological processes and volcanological tools. J Volcanol Geotherm Res 1: 3–33

Anderson AT (1979) Water in some hypersthenic magmas. J Geol 87: 509–531

Anderson CA (1941) Volcanoes of the Medicine Lake Highland, California. University of California Publications, Bulletin of Department of Geological Sciences. 25, no. 7: 347–422

Arculus RJ, Wills KJ (1980) The petrology of igneous blocks and inclusions from the lesser Antilles island arc. J Petrol 21: 143–168

Baedecker PA (1987) Methods for geochemical analysis. US Geol Sun Bull 1770

Baker MB, Grove TL, Kinzler RJ, Donnelly-Nolan JM, Wandless GA (1991) Origin of compositional zonation (high-alumina basalt to basaltic andesite) in the Giant Crater lava field, Medicine Lake volcano, northern California. J Geophys Res 96(B13): 21819–21842

Bartels KS, Kinzler RJ, Grove TL (1991) High pressure phase relations of primitive high-alumina basalts from Medicine Lake volcano, northern California. Contrib Mineral Petrol 108: 253–270

Bence AB, Albee AL (1968) Empirical corrections factors for the electron microanalysis of silicates and oxides. J Geol 76: 382–403

Boettcher AL (1973) Volcanism and orogenic belts – the origin of andesites. Tectonophysics 17: 223–240

Brophy JG (1989) Basalt convection and plagioclase retention: a model for the generation of high-alumina arc basalt. J Geol 97: 319–329

Crawford AJ, Falloon TJ, Eggins S (1987) The origin of island arc high-alumina basalts. Contrib Mineral Petrol 97: 417–430

Donnelly-Nolan JM, Champion DE, Miller CD, Grove TL, Trimble DA (1990) Post-11,000-year volcanism at Medicine Lake Volcano, Cascade Range, northern California. J Geophys Res 95: 19693–19704

Donnelly-Nolan JM, Champion DE, Grove TL, Baker MB, Taggart JE, Bruggman PE (1991) The Giant Crater lava field: geology and geochemistry of a compositionally zoned, high-alumina basalt to basaltic andesite eruption at Medicine Lake volcano, California. J Geophys Res 96(B13):21843–21863

Draper DS, Johnston AD (1992) Anhydrous PT phase relations of an Aleutian high-MgO basalt: an investigation of the role of olivine-liquid reaction in the generation of arc high-alumina basalts. Contrib Mineral Petrol 112(4):501–519

Dzurisin D, Donnelly-Nolan JM, Evans JR, Walter SR (1991) Crustal subsidence, seismicity and structure near Medicine Lake volcano, California. J Geophys Res 96: 16319–16333

Eichelberger JC (1975) Origin of andesite and dacite: evidence of mixing at Glass Mountain in California and other circum-Pacific volcanoes. Geol Soc Am Bull 86: 1381–1391

Ewart A (1982) The mineralogy and petrology of Tertiary-recent orogenic volcanic rocks with special reference to the andesitic-basaltic compositional range. In: Thorpe RS (ed) Andesites. Wiley, New York, pp 25–95

Fujimaki H, Tatsumoto M, Aoki K (1984) Partition coefficients of Hf, Zr and REE between phenocrysts and groundmass. J Geophys Res 89: 662–672

Gaetani GA, Grove TL, Bryan WB (1993) The influence of water on the petrogenesis of subduction related igneous rocks. Nature 365: 332–334

Gerlach DC, Grove TL (1982) Petrology of Medicine Lake Highland volcanics: characterization of the endmembers of magma mixing. Contrib Mineral Petrol 80: 147–159

Gill JB (1981) Orogenic andesites and plate tectonics. Springer, Berlin Heidelberg

Grove TL (1993) Corrections to expressions for calculating mineral components in "Origin of calc-alkaline series lavas at Medicine Lake volcano by fractionation, assimilation and mixing" and "Experimental petrology of normal MORB near the Kane Fracture Zone: 22°–25°N, mid-Atlantic ridge". Contrib Mineral Petrol 114: 422–424

Grove TL, Bryan WB (1983) Fractionation of pyroxene-phyric MORB at low pressure: an experimental study. Contrib Mineral Petrol 84: 293–309

Grove TL, Kinzler RJ, Baker MB, Donnelly-Nolan JM, Lesher CE (1988) Assimilation of granite by basaltic magma at Burnt Lava flow, Medicine Lake volcano, northern California. Contrib Mineral Petrol 99: 320–343

Gust DA, Perfit MR (1987) Phase relations of a high-Mg basalt from the Aleutian Island arc: implications for primary island arc basalts and high-Al basalts. Contrib Mineral Petrol 97: 7–18

Housh TB, Luhr JF (1991) Plagioclase-melt equilibria in hydrous systems. Am Mineral 76: 477–492

Kay SM, Kay RW, Citron GP (1982) Tectonic controls on tholeiitic and calc-alkaline magmatism in the Aleutian arc. J Geophys Res 87: 4051–4072

Powers HA (1932) The lavas of the Modoc Lava-Bed Quadrangle. Am Mineral 17: 253–294

Ringwood AE (1974) The petrological evolution of island arc systems. J Geol Soc London 130: 183–204

Roeder PL, Emslie RF (1970) Olivine liquid equilibrium. Contrib Mineral Petrol 29: 275–289

Rose WI, Anderson AT Jr, Woodruff LG, Bonis SB (1978) The October 1974 basaltic tephra from Fuego volcano: description and history of the magma body. J Volcanol Geotherm Res 4: 3–53

Sisson TW, Grove TL (1993a) Experimental investigations of the role of H_2O in calc-alkaline differentiation and subduction zone magmatism. Contrib Mineral Petrol 113: 143–166

Sisson TW, Grove TL (1993b) Temperatures and H_2O contents of low-MgO high-alumina basalts. Contrib Mineral Petrol 113: 167–184

Sisson TW, Layne GD (1993) H_2O in basalt and basaltic andesite glass inclusions from four subduction-related volcanoes. Earth Planet Sci Lett 117: 619–635

Taggart JEJ, Lindsay JR, Scott BA, Vivit DV, Bartel AJ, Stewart KC (1987) Analysis of geologic materials by a wavelength dispersive X-ray fluorescence spectrometry. US Geol Surv Bull 1170: E1–E9

Yoder HS (1965) Diopside-anorthite-water at five and ten kilobars and its bearing on explosive volcanism. Carnegie Inst Washington Yearb 64: 82–89

Yoder HSJ (1969) Calc-alkaline andesites: experimental data bearing on the origin of their assumed characteristics. Oreg Dep Geol Miner Res Bull, Proc Andesite Conference: 77–91